An Automated Method of MFRSR Calibration for Aerosol Optical Depth Analysis with Application to an Asian Dust Outbreak over the United States

JOHN A. AUGUSTINE

National Oceanic and Atmospheric Administration/Air Resources Laboratory/Surface Radiation Research Branch, Boulder, Colorado

CHRISTOPHER R. CORNWALL AND GARY B. HODGES

Cooperative Institute for Research in the Environmental Sciences, University of Colorado, Boulder, Colorado

CHARLES N. LONG

Atmospheric Radiation Measurement Program, Pacific Northwest National Laboratory, Richland, Washington

CARLOS I. MEDINA

Department of Engineering, Colorado School of Mines, Golden, Colorado

JOHN J. DELUISI

National Oceanic and Atmospheric Administration/Air Resources Laboratory/Surface Radiation Research Branch, Boulder, Colorado

(Manuscript received 10 January 2002, in final form 27 August 2002)

ABSTRACT

Over the past decade, networks of Multifilter Rotating Shadowband Radiometers (MFRSR) and automated sun photometers have been established in the United States to monitor aerosol properties. The MFRSR alternately measures diffuse and global irradiance in six narrow spectral bands and a broadband channel of the solar spectrum, from which the direct normal component for each may be inferred. Its 500-nm channel mimics sun photometer measurements and thus is a source of aerosol optical depth information. Automatic data reduction methods are needed because of the high volume of data produced by the MFRSR. In addition, these instruments are often not calibrated for absolute irradiance and must be periodically calibrated for optical depth analysis using the Langley method. This process involves extrapolation to the signal the MFRSR would measure at the top of the atmosphere ($I_{\lambda 0}$). Here, an automated clear-sky identification algorithm is used to screen MFRSR 500-nm measurements for suitable calibration data. The clear-sky MFRSR measurements are subsequently used to construct a set of calibration Langley plots from which a mean $I_{\lambda 0}$ is computed. This calibration $I_{\lambda 0}$ may be subsequently applied to any MFRSR 500-nm measurement within the calibration period to retrieve aerosol optical depth. This method is tested on a 2-month MFRSR dataset from the Table Mountain NOAA Surface Radiation Budget Network (SURFRAD) station near Boulder, Colorado. The resultant $I_{\lambda 0}$ is applied to two Asian dust–related high air pollution episodes that occurred within the calibration period on 13 and 17 April 2001. Computed aerosol optical depths for 17 April range from approximately 0.30 to 0.40, and those for 13 April vary from background levels to >0.30. Errors in these retrievals were estimated to range from ± 0.01 to ± 0.05, depending on the solar zenith angle. The calculations are compared with independent MFRSR-based aerosol optical depth retrievals at the Pawnee National Grasslands, 85 km to the northeast of Table Mountain, and to sun-photometer-derived aerosol optical depths at the National Renewable Energy Laboratory in Golden, Colorado, 50 km to the south. Both the Table Mountain and Golden stations are situated within a few kilometers of the Front Range of the Rocky Mountains, whereas the Pawnee station is on the eastern plains of Colorado. Time series of aerosol optical depth from Pawnee and Table Mountain stations compare well for 13 April when, according to the Naval Aerosol Analysis and Prediction System, an upper-level Asian dust plume enveloped most of Colorado. Aerosol optical depths at the Golden station for that event are generally greater than those at Table Mountain and Pawnee, possibly because of the proximity of Golden to Denver's urban aerosol plume. The dust over Colorado was primarily surface based on 17 April. On that day, aerosol optical depths at Table Mountain and Golden are similar but are 2 times the magnitude of those at Pawnee. This difference is attributed to meteorological conditions that favored air stagnation in the planetary boundary layer along the Front Range, and a west-to-east gradient in aerosol concentration. The magnitude and timing of the aerosol optical depth measurements at Table Mountain for these events are found to be consistent with independent measurements made at NASA Aerosol Robotic Network (AERONET) stations at Missoula, Montana, and at Bondville, Illinois.

1. Introduction

When considering the myriad of climate forcing parameters, the effects of aerosols on climate change have been shown to be commensurate in magnitude but opposite to that of increased carbon dioxide (Hansen et al. 2000). Individually, however, different types of aerosols can have differing effects on temperature. Some, such as black carbon, absorb solar radiation and warm the atmosphere, whereas others, for example, volcanic aerosols in the stratosphere, primarily scatter solar ra-

Corresponding author address: John A. Augustine, NOAA/Air Resources Laboratory, R/ARL, 325 Broadway, Boulder, CO 80305.
E-mail: john.a.augustine@noaa.gov

diation and may have a cooling effect because they reflect some of the incoming solar radiation back to space. It is well documented that the earth's climate temporarily cooled following the major volcanic eruptions of the last century (Dutton and Christy 1992; Hansen et al. 1992). Aerosols may also have an indirect effect on climate by changing the radiative properties of clouds (Charlson et al. 1992). Owing to the contrasting effects that aerosols can have on climate, Hansen et al. (2000) conclude that ''unless climate forcings by all aerosols are precisely monitored, it will be difficult to define optimum [climate] policies.''

Systematic monitoring of atmospheric turbidity in the United States began with the Volz sun photometer network in 1961 (Flowers et al. 1969). That effort ended in 1966. During the past decade several new aerosol monitoring networks have emerged. These differ from the Volz network, which employed hand-held sun photometers, by relying on robotic instruments. One such network is the National Aeronautics and Space Administration (NASA) Aerosol Robotic Network (AERONET; Holben et al. 2001), which commenced operation in 1993 and employs the Cimel CE 318-1 automated sun photometer. International in scope, AERONET's U.S. complement has grown to about 20 stations. Other U.S. networks employ the Multifilter Rotating Shadowband Radiometer (MFRSR) (Harrison et al. 1994). These include the National Oceanic and Atmospheric Administration's (NOAA) Surface Radiation Budget Network (SURFRAD; Augustine et al. 2000), the U.S. Department of Agriculture (USDA) UV monitoring network (Bigelow et al. 1998), the Department of Energy (DOE) Atmospheric Radiation Measurement Program (ARM) Southern Great Plains site (Stokes and Schwartz 1994), and the Quantitative Links program (Michalsky et al. 2001).

Instrument automation introduces an additional level of data processing over manually obtained sun photometer data. The new robotic instruments such as the MFRSR are unattended and are usually operated in remote areas. Thus, their basic data represent a wide range of atmospheric conditions, most of which are undesirable for an aerosol optical depth (AOD) analysis, for example, when clouds obscure the sun. Furthermore, MFRSRs are typically not calibrated against standard references and therefore must be calibrated in a relative sense from their own operational data before they can be reliably used for AOD retrievals. The usual method of calibration is the Langley plot technique (Shaw 1983) in which the instrument's inferred direct normal signal is extrapolated to the top of the atmosphere ($I_{\lambda 0}$). Once a stable $I_{\lambda 0}$ for an MFRSR channel is computed, it may be used for AOD retrievals within the calibration period. Identification of $I_{\lambda 0}$ for MFRSR channels must be done regularly to account for sensor and filter drift, periodic changes in the solar output, and variations in the earth–sun distance. To develop a system of recurrent redefinition of $I_{\lambda 0}$ without employing an automatic screening aid to select periods appropriate for the calibration exercise is time consuming and inefficient.

Here, we apply the method of Long and Ackerman (2000) to broadband solar component data to identify clear-sky and nonhazy periods. These times are used as guidance to select MFRSR data for calibration Langley plots. Our hypothesis is that several of these ''clear-sky'' Langley plots within a several-week-long period would provide a stable sample of zero air mass extrapolations ($I_{\lambda 0}$) from which a reliable mean may be computed. This mean $I_{\lambda 0}$ is a stable, but transient calibration that applies only to the MFRSR for which it was computed. It may be combined with any I_λ measurement from that particular MFRSR within the calibration period to compute AOD. This method of calibration is tested on a 2-month period using data from the Table Mountain, Colorado, SURFRAD station. The resultant calibration $I_{\lambda 0}$ is subsequently applied to two high air pollution events that were associated with an Asian dust outbreak. Resultant AOD retrievals are verified by comparing them to nearby independent measurements.

2. Determination of aerosol optical depth

Aerosol optical depth is determined from spectral solar measurements through application of a form of Beer's law (1)

$$I_\lambda = I_{\lambda 0} \exp\left[-m \sum \tau(\lambda)\right], \tag{1}$$

where I_λ is the direct normal irradiance at the surface for wavelength λ, $I_{\lambda 0}$ is the extraterrestrial direct normal irradiance for λ, m is the optical path through a curved atmosphere, and $\Sigma\ \tau$ is the total optical depth of the atmosphere for radiation at wavelength λ. Note that in applying (1), a calibration constant C to convert measured voltage to irradiance, that is, $I_\lambda = CV_\lambda$, is not necessary because the constant would be applied to voltage signals on each side of the equation and thus would cancel. Because we do not apply calibration constants to measured MFRSR voltage signals, from here on, references to MFRSR signals, that is, I_λ and the extrapolated extraterrestrial value $I_{\lambda 0}$, actually refer to voltages.

Generally, optical depth for a particular atmospheric constituent is described as

$$\tau(\lambda) = \int_{z=0}^{\infty} \alpha x(z)\, dz, \tag{2}$$

where α is the extinction coefficient for wavelength λ, x is the density of the constituent, and z is the height above the surface.

The linearized form of Beer's Law is more easily interpreted:

$$\ln I_\lambda = -m \sum \tau(\lambda) + \ln I_{\lambda 0}. \tag{3}$$

From (3) it is understood that the slope of a plot of the natural log of the measured signal at the surface at nor-

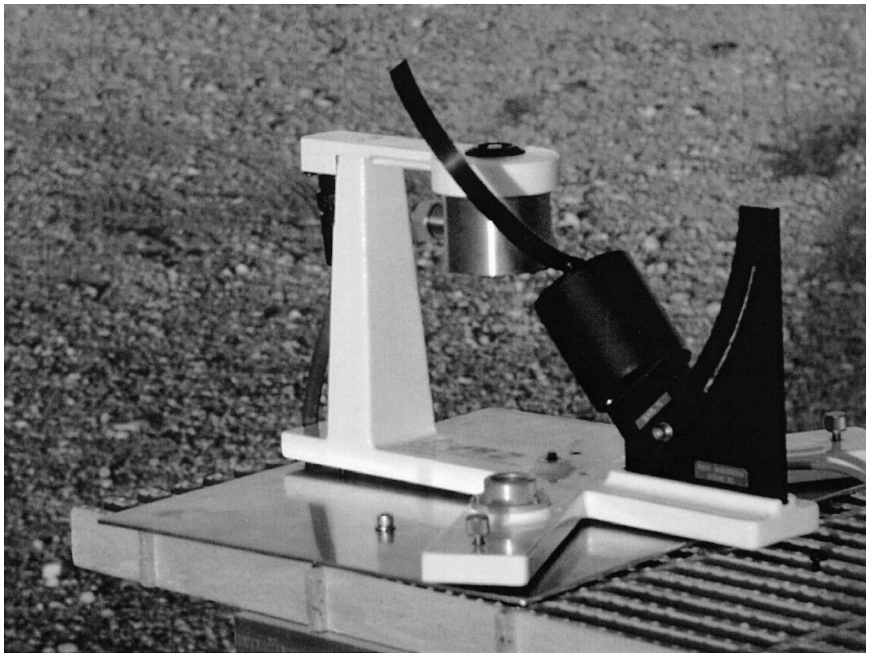

FIG. 1. The Multifilter Rotating Shadowband Radiometer.

mal incidence to the sun ($\ln I_\lambda$), versus m, the optical path length, is the total optical depth ($\Sigma\ \tau$) of the atmosphere, and that the y intercept ($\ln I_{\lambda 0}$) is the natural log of the extraterrestrial signal for wavelength λ. To extract total optical depth information from these Langley plots, measurements of I_λ must be made for various optical pathlengths, that is, at different times of day. In this analysis, optical path (m) is computed using an approximation of the Chapman function described in Smith and Smith (1972).

The total optical depth ($\Sigma\ \tau$) recovered from 500-nm measurements is primarily made up of contributions from aerosols (τ_a), molecular (Rayleigh) scattering (τ_R), and small components from ozone absorption (τ_o) and nitrogen dioxide (NO_2) absorption (τ_N). Although NO_2 is more active in the ultraviolet, it does absorb in the visible wavelengths. At background levels of concentration, its contribution to the total optical depth at 500 nm is negligible, but for high air pollution events it should be considered. According to Davidson et al. (1988), τ_N is a function of the absorption cross section of NO_2 at 500 nm, the ambient concentration of NO_2, and the depth of the planetary boundary layer (PBL).

The contribution from molecular scattering is parameterized by

$$\tau_R = 0.0088[\lambda^{(-4.15+0.2\lambda)}]\frac{p}{p_0}, \tag{4}$$

as reported by Marggraf and Griggs (1969), where λ is the wavelength of the measurements (μm), and p and p_0 are the station pressure and the mean sea level pressure, respectively. Dutton et al. (1994) report that the contribution to the total optical depth from ozone absorption (τ_o) at 500 nm is 0.0087 times the observed total ozone amount divided by a reference value of 330 Dobson units. To obtain the fraction of the total optical depth contributed by aerosols (τ_a), the parts contributed by molecular scattering, and ozone and NO_2 absorption must be removed from the total, as shown by

$$\tau_a = \sum \tau - \tau_R - \tau_o - \tau_N. \tag{5}$$

3. The MFRSR

Components of the MFRSR (Fig. 1) pertinent to this discussion are the horizontal circular aperture covered by a white diffuser disk, and the rotating shadowband that intermittently shades the diffuser. A global measurement is made while the shadowband is at rest outside the instrument's field of view. The diffuse measurement is made when the shadowband rotates to a position such that it shades the diffuser disk. Thus, the MFRSR alternately measures global and diffuse irradiance impinging on a horizontal surface. Accurate positioning of the band is controlled by an ephemeris calculation. This instrument is designed to minimize measurement errors caused by the exclusion angle of the shadowband. During the band's rotation it stops three times: 1) just before the shadow shades the disk, 2) with its shadow over the diffuser disk, and 3) with its shadow on the other side of the disk. Measurements made when the shadow is on either side of the diffuser are used to estimate the fraction of diffuse irradiance blocked by the shadowband when the disk is shaded, which is then

added back into the diffuse measurement. The horizontal component of the direct beam is inferred by subtracting the corrected diffuse measurement from the global measurement. The direct component at normal incidence to the sun is computed by dividing the horizontal component of the direct beam by the cosine of the solar zenith angle, which is accurately provided by the ephemeris calculation. In this way, an MFRSR mimics direct normal measurements of a sun photometer. For more details on the MFRSR, see Harrison et al. (1994).

MFRSRs used at SURFRAD stations are programmed to sample at 15-s intervals and to provide 2–min averages. Radiation that passes through the diffuser disk is received simultaneously by seven silicon sensors: a total solar channel and six spectral channels that measure irradiance in 10-nm-wide bands ranging from the ultraviolet to the near infrared, peaking nominally at 415, 500, 615, 670, 870, and 940 nm. In processing MFRSR data, measured signals are corrected for the cosine error of the instrument as documented by the manufacturer; however, these characteristics may change as the instrument ages.

4. Method

Equations (3) and (5) dictate that the slope of a Langley plot is the total atmospheric optical depth, from which the AOD may be extracted. However, several factors increase the uncertainty of a single Langley plot's slope, for example, a change in aerosol concentrations over the course of the day, effects of atmospheric noise such as that from subvisual cirrus (Shaw 1976), and instrument errors. Also, Harrison et al. (1994) report that the relatively large field of view of an MFRSR makes it vulnerable to the adverse effects of enhanced forward scattering by aerosols or thin cirrus cloud particles whose dimensions are large compared to the wavelength of the measurement. These enhanced signals artificially decrease the inferred total optical depth. Such problems suggest that a single Langley plot for a particular morning or afternoon may not provide accurate AOD information.

It is best to establish a mean calibration $I_{\lambda 0}$ that is representative of a several-week period surrounding a particular event for which an AOD analysis is desired. Once established, this value can serve as the instrument's calibration for optical depth analysis for that period. However, periodic $I_{\lambda 0}$ calibration throughout the year is necessary because the extraterrestrial signal will slowly change owing to filter drift and periodic changes in the earth–sun distance. To reduce uncertainty when computing $I_{\lambda 0}$, only times of good air quality and unobscured views of the solar disk should be used. This procedure is common. For example, in the method used for the Quantitative Links program (Michalsky et al. 2001), the 20 most-linear Langley plots over a 6-week period are chosen, each of which is made up of measurements with a clear view of the solar disk. Before computing a representative calibration $I_{\lambda 0}$, they further pare those 20 to 10 using an objective method reported by Forgan (1988). The method of Harrison and Michalsky (1994), which has been automated for application to visible MFRSRs in the USDA UV network, uses statistical filters to choose data for calibration Langley plots, and applies linear regression to determine $I_{\lambda 0}$. Other methods of Langley plot calibration have been reported, for example, Shaw (1976) and Reagan et al. (1984), but most involve a manual selection of calibration data representing the clearest skies and radiatively stable conditions. More recently, Alexandrov et al. (2002) have developed a comprehensive method of MFRSR data analysis to calibrate all channels of the instrument, as well as to retrieve aerosol properties, and column amounts of NO_2 and ozone.

Harrison and Michalsky (1994) state that ''the simple minded notion of using a least squares regression on all [MFRSR] data works only under true clear-sky conditions.'' Here, we apply that principle by selecting MFRSR data for calibration Langley plots using the clear-sky detection algorithm of Long and Ackerman (2000) as guidance. The Long and Ackerman algorithm operates on broadband solar component (direct plus diffuse) data and uses empirical means to determine clear-sky periods. The broadband solar data may be provided by an MFRSR's broadband channel or by collocated independent solar component measurements, such as those from a SURFRAD station. However, to apply the clear-sky detection algorithm to MFRSR data alone, its broadband channel must be calibrated for absolute irradiance. For this purpose, high accuracy is not necessary. Temporarily running a calibrated pyranometer alongside an MFRSR to transfer a nominal calibration to its broadband channel is all that is necessary for the method described here to be viable for a standalone MFRSR.

The Long and Ackerman (2000) clear-sky detection algorithm is completely automated; only the period to be processed is specified. The method employs four sequential tests that scrutinize total solar (direct plus diffuse) and diffuse solar irradiance to detect cloud-free skies. These tests are based on the premise that cloudy and hazy skies exhibit characteristics in the components of downwelling shortwave irradiance that clear skies do not. The first two tests eliminate periods of obvious cloudiness by comparing normalized transformations of the total and diffuse solar measurements to expected clear-sky limits. The other two tests examine temporal variations of parameters computed from the total and diffuse solar irradiance to eliminate more subtle periods of thin cloud or hazy conditions. While each test alone will not detect every clear-sky period, the net of all four represents a fairly complete screening. Identified periods correspond to conditions of cloud-free skies for an effective 160° field of view centered on the zenith. Sample results for a day of SURFRAD data are shown in Fig.

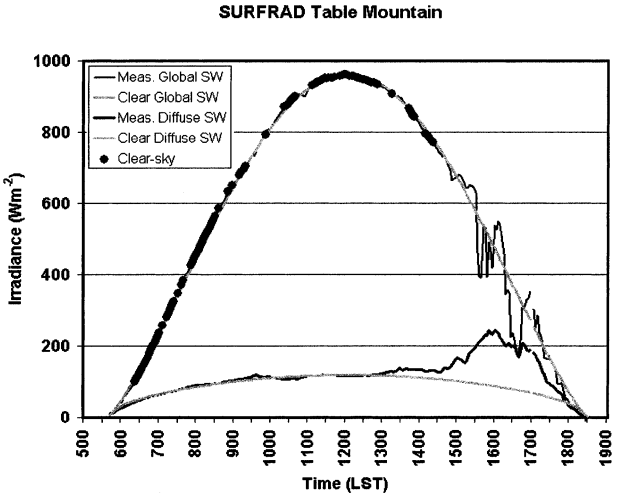

FIG. 2. Clear-sky identification results for 9 Apr 2001 at Table Mountain, CO. Black curves represent the actual global and diffuse solar measurements. Black dots indicate times that were determined to be cloud-free by the Long and Ackerman (2000) algorithm. Gray curves are empirical daily fits to the clear-sky global solar and diffuse solar measurements.

2. The points marked by black dots are times identified as clear.

If a sufficient number of clear periods are detected, the Long and Ackerman method will also empirically fit the locus of clear-sky total, direct, and diffuse solar irradiance separately to daily envelopes of normally expected clear-sky irradiance for those parameters, for example, the gray lines in Fig. 2. The method interpolates clear-sky envelopes to days for which such empirical fits are not possible. The difference between an irradiance measurement and its corresponding point on the clear-sky envelope for a particular time represents accurate solar forcing owing to clouds or aerosols at that time. This feature is utilized to compute the effects of aerosols on the downwelling solar irradiance for the two high air pollution days analyzed in section 6.

The advantage of using only clear-sky MFRSR data for calibration Langley plots is that noise is reduced and a confident extrapolation to $\ln(I_{\lambda 0})$ by simple linear regression is feasible. Only those Langley plots with 20 or more clear-sky points are retained for the calibration exercise. Constructing several of these clear-sky Langley plots over a several-week period produces a pool of extrapolated $\ln(I_{\lambda 0})$ values for which a reliable mean is computed. Because the Long and Ackerman clear-sky detection method depends on minimum levels of, and the temporal stability of, diffuse solar irradiance, its use to screen MFRSR data for calibration periods increases confidence that the mean, or calibration $I_{\lambda 0}$ will be stable and free of any effects that promote increases in diffuse solar radiation, for example, high aerosol content or cirrus clouds. After a calibration $I_{\lambda 0}$ is established, it may be applied to any I_λ measurement within the calibration period as the anchor point of a two-point Langley plot from which an AOD may be retrieved. Accordingly, application to a series of MFRSR measurements would provide a time series of AOD. According to Harrison et al. (1994), any adverse effects from cirrus clouds or subvisual cirrus would appear as noise in such a series, and thus would be easily distinguished from the more stable AOD signal. Although 500-nm channel data are utilized here, the calibration method described is applicable to any MFRSR channel.

5. Calibration of the MFRSR at the Table Mountain SURFRAD station

a. Determination of the mean $I_{\lambda 0}$

A 2-month period from late March through late May of 2001 encompassing two high air pollution events on 13 and 17 April 2001 was used to establish a calibration $I_{\lambda 0}$ for the Table Mountain MFRSR's 500-nm channel. Within this period, SURFRAD broadband solar data were analyzed using the Long and Ackerman (2000) method. Fourteen days were determined to have a sufficient number of clear-sky periods to be used for calibration Langley plots. Four of the days had both clear mornings and clear afternoons, nine had only clear mornings, and one had only a clear afternoon. Individual clear-sky Langley plots for these 18 periods were used to determine a representative calibration $I_{\lambda 0}$ for the MFRSR's 500-nm channel. Figure 3 shows a plot from this sample. The solid points represent clear-sky screened MFRSR measurements; note that they form a nearly linear path with little variation. The line shown represents a least squares fit to the screened (solid) points only. Without clear-sky guidance, the slope and intercept of the best fit line would likely have been different, even if the obvious outliers were disregarded. Because of the clear-sky identification method's sensitivity to higher than normal diffuse radiation, the problem posed by varying concentrations of aerosols adding uncertainty to the slope and *y* intercept of a calibration Langley plot is minimized. In Fig. 3, note that the MFRSR data for solar pathlengths six through eight exhibit the problem of a changing slope, but those points were not identified as clear, and thus were not used in determining $I_{\lambda 0}$ for that plot. The other 17 clear-sky calibration Langley plots were similarly linear and exhibited little scatter.

Table 1 lists the properties of the 18 calibration Langley plots. The slope and *y* intercept of each were determined by applying linear regression to clear-sky screened MFRSR data. In computing the mean *y* intercept ($\ln I_{\lambda 0}$), each was weighted according to the number of clear-sky points in the plot. Weighted averaging was used because it was assumed that the extrapolated *y* intercept of an individual Langley plot would be more reliable if more clear-sky points were used for the linear regression. Morning and afternoon *y* intercepts from this sample were not averaged separately. The average

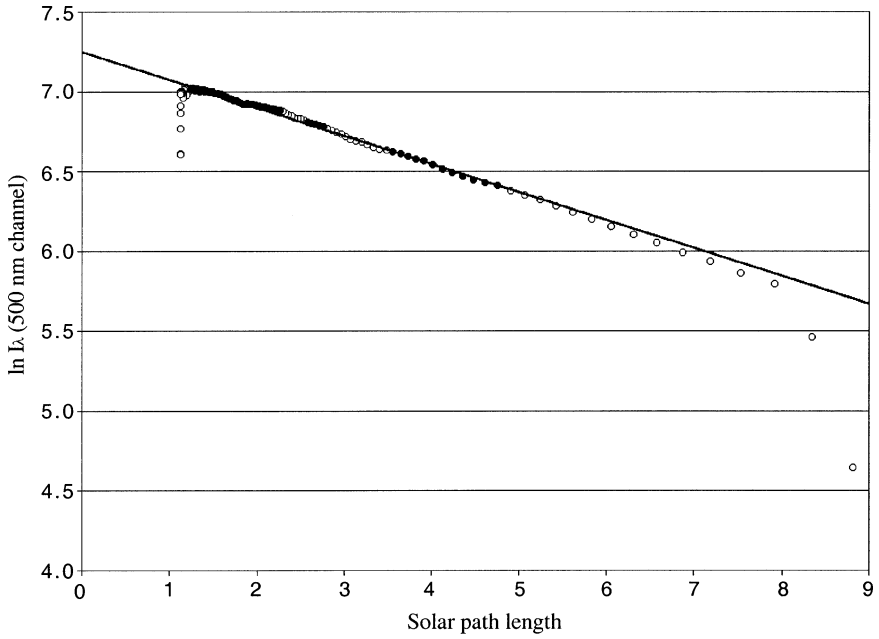

FIG. 3. Langley plot for the MFRSR 500-nm channel at Table Mountain SURFRAD station the morning of 23 Apr 2001. Solid circles represent time periods identified as clear by the Long and Ackerman (2000) method. The line is the least squares linear fit to the solid (clear sky) points only.

$\ln(I_{\lambda 0})$ and standard deviation for the 2-month calibration period was 7.38 ± 0.057. The small standard deviation (±0.8%) lends-confidence to the validity of the mean value and its subsequent application to the two high air pollution events.

A sensitivity test was carried out in which the clear-sky guidance was ignored. Daily Langley plots for the 2-month period were examined visually for good candidates for a subjective calibration analysis. Only those plots that were perceived to be clearest (most linear) were considered. Langley plots from 17 mornings and 10 afternoons were determined to be of sufficient quality. Lines were subjectively drawn to fit these data and those lines were manually extrapolated to the *y* intercept. Measurements showing obvious cloud contamination, and those from very early and late daylight periods that showed cosine-type errors (changing slope) were ignored. The mean $\ln(I_{\lambda 0})$ and standard deviation from this sample was 7.40 ± 0.054. This value is not statistically different from the result derived using clear-sky guidance and thus lends further confidence to the results of the automated algorithm.

TABLE 1. The $\ln(I_{\lambda 0})$ extrapolations and total optical depth for selected ''clear-sky'' days.

Date	No. of clear points	Extrapolated $\ln(I_{\lambda 0})$ (*y* intercept)	Total optical depth, $\Sigma\tau$ (slope)
Morning			
23 Mar 2001	50	7.45	0.19
9 Apr 2001	150	7.38	0.27
23 Apr 2001	95	7.26	0.18
24 Apr 2001	29	7.24	0.17
25 Apr 2001	141	7.39	0.24
26 Apr 2001	186	7.39	0.24
7 May 2001	187	7.38	0.26
8 May 2001	191	7.37	0.21
13 May 2001	177	7.39	0.28
14 May 2001	43	7.40	0.26
20 May 2001	21	7.40	0.20
21 May 2001	72	7.34	0.18
22 May 2001	55	7.34	0.16
Afternoon			
31 Mar 2001	21	7.42	0.25
25 Apr 2001	126	7.38	0.30
26 Apr 2001	171	7.48	0.34
7 May 2001	45	7.35	0.32
8 May 2001	133	7.36	0.22

b. Determination of the background aerosol optical depth

The mean slope of the 18 clear-sky calibration Langley plots of 0.25 ± 0.05 represents the background total optical depth ($\Sigma\ \tau$) for the 2-month calibration period. This value was also computed by weighted average. Individual slopes from this sample range from 0.16 to 0.34 (see Table 1) and exhibit a standard deviation of 20%, which is much greater than the 0.8% standard deviation of the *y* intercepts. This larger variation is not unexpected because the aerosol content of the atmosphere changes naturally even for the cloud-free, non-hazy periods used in this calibration exercise. Also note in Table 1 that the afternoon total optical depths are

generally greater than the morning values, but this too is expected because aerosol concentrations usually grow with the increased turbulence associated with the building of the daytime boundary layer, and with solar-driven photochemical processes. Regardless of this difference, the morning and afternoon slopes were grouped together in computing the mean background total optical depth.

To extract the background AOD from the total, the contributions owing to molecular scattering and ozone absorption were removed using (5). The mean surface pressure at Table Mountain and a representative ozone amount of 300 Dobson units were assumed in computing these quantities. Because the periods used for the calibration Langley plots were characterized by clear skies and nonhazy conditions, the contribution to the total optical depth by NO_2 absorption, which becomes significant only during high air pollution events, was assumed to be negligible. These results indicate a mean background AOD of 0.12 ± 0.05 for the 2-month period. This value is slightly more than half of the mean AOD value of 0.23[1] for April in Boulder, Colorado, reported by Flowers et al. (1969), which is the annual maximum for Boulder. However, their value for April encompasses all events, including outbreaks of Asian dust, which are common during that time of year (Husar et al. 2001; Parungo et al. 1994; Uematsu et al. 1983). Screening MFRSR data using clear-sky guidance would exclude days having high aerosol content because of the Long and Ackerman method's sensitivity to the intensity and variations of diffuse solar irradiance. For example, long periods of 13 and 17 April were cloudless, but neither is listed in Table 1; the clear-sky identification algorithm rejected all but one 3-min period on those days. The fact that mean background AOD computed from the 18 clear-sky calibration periods is similar to the annual minimum for Boulder of ~0.09 reported by Flowers et al. (1969) is consistent with the relatively clean periods that were used in the calibration analysis. It should be noted that the background AOD has no application to the calibration of the MFRSR; it was computed only as a reference with which to gauge AOD values derived for the two high air pollution events.

6. Testing the method

a. The high air pollution events of April 2001

1) WEATHER CONDITIONS

Two high air pollution events that occurred over the Front Range of Colorado on 13 and 17 April 2001 were chosen to test the method of MFRSR calibration and AOD analysis described here. On 17 April, meteorological conditions over the Front Range region were conducive to the trapping of boundary layer air. The surface weather in eastern Colorado (Fig. 4) was dominated by an elongated north-to-south high pressure system centered to the east that extended from Manitoba to northern Texas, and a stationary front on the western periphery of the high that was stalled along the Front Range of the Rocky Mountains from New Mexico to Canada. Light south-southeasterly winds behind the front kept it positioned against the Front Range. Figure 5 shows the Denver rawinsonde plot for the morning of 17 April 2001. The strong temperature inversion just below the 700-hPa level, in combination with light winds in the boundary layer would act to trap aerosols close to the surface. The 0000 UTC 18 April sounding later that day (not shown) shows that the capping inversion never broke, nor did it elevate during the day. Furthermore, gentle surface flow from the south-southeast associated with the high pressure and stationary front acted to keep the vertically trapped surface aerosols close to the foothills. On 13 April, a low-level inversion was present in the morning Denver sounding, but the afternoon sounding showed the boundary layer to be well mixed to 500 hPa, indicating that the low-level inversion broke during the day. Surface weather conditions on 13 April were characterized by a lee trough and more typical westerly flow over the Front Range in the early morning, turning to light southerly flow in the afternoon.

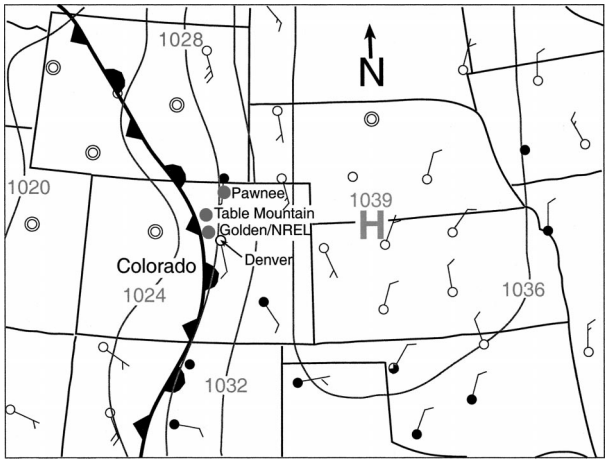

FIG. 4. Surface weather for 1500 UTC 17 Apr 2001. Small circles are National Weather Service surface stations. An open circle indicates clear skies, solid is overcast, and partial shading indicates partly cloudy conditions. Wind vectors indicate the direction from which the wind is coming, and the barbs at the end of the vectors depict wind speed. A full barb is 5 m s^{-1}, a half barb is 2.5 m s^{-1}, and a concentric circle with no vector represents calm conditions. Gray contours are isobars of surface pressure (hPa) reduced to sea level. Stations where aerosol optical depth measurements were made are shown as large solid gray circles labeled with the station names.

2) AEROSOL DISTRIBUTION

An ensemble analysis of the global distribution of aerosols was constructed by the Navy Aerosol Analysis

[1] The turbidity values reported in Flowers et al. (1969) were computed using a log base 10 version of Beer's law. Their reported annual turbidity maximum for Boulder is actually 0.10. Converting this value to log base *e* results in an aerosol optical depth value of 0.23.

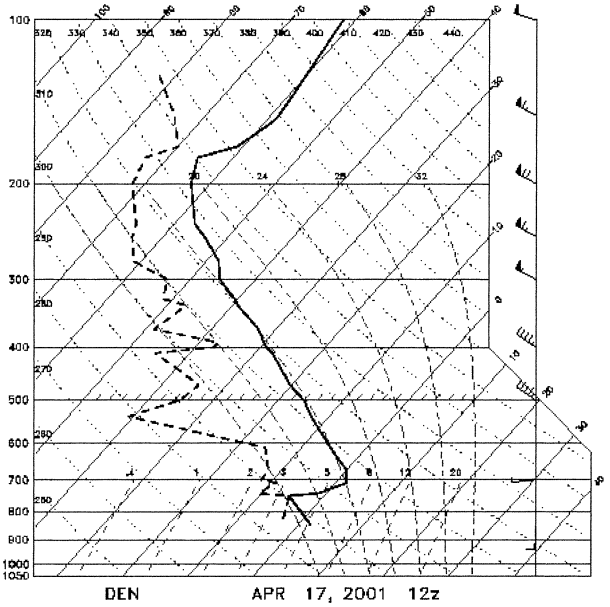

FIG. 5. Rawinsonde sounding for Denver, CO, for 1200 UTC 17 Apr 2001 on a skew *T*–log*p* background. The thick dark solid and dashed lines are the temperature and dewpoint temperature profiles, respectively. Mandatory-level winds shown at right. A flag represents 25 m s^{-1}, a full barb is 5 m s^{-1}, and a half barb is 2.5 m s^{-1}. The orientation of the vector indicates the direction from which the wind is coming. On the skew *T*–log*p* background, lines of constant temperature (°C) are labeled at right and across the top, and lines of constant pressure (hPa) are labeled at left.

and Prediction System (NAAPS) for these events. It indicates that an upper-level Asian dust cloud enveloped most of Colorado on 13 April; however, by 17 April it had drifted to the eastern United States, leaving no measurable Asian dust at upper levels over Colorado. The NAAPS diagnostics for surface aerosols depict a scenario contrary to that at upper levels. On 17 April, surface concentrations of dust were very high all day along the Front Range of the Rocky Mountains from New Mexico to Montana. This is consistent with the strong low-level trapping inversion and south-southeasterly surface flow behind the stationary front that persisted throughout that day. On 13 April, when the Asian dust cloud was present at upper levels over Colorado, the NAAPS analysis shows the surface aerosol concentration to be negligible in the morning but increasing in the afternoon.

b. Calculation of τ_R, τ_o, and τ_N

According to (4), the total optical depth owing to molecular scattering at 500 nm (τ_R) for Table Mountain's station pressure on 13 April (828 hPa) was 0.119, and that for 17 April (837 hPa) was 0.120. Total ozone was measured at Boulder several times between 1000 and 1400 local standard time (LST) on both days using a Dobson instrument. Values on 13 April ranged from 330 to 345 Dobson units, with a mean of 336. Ozone amounts on 17 April ranged from 310 to 315 Dobson units, with a mean of 313. Using the mean ozone amounts, optical depths owing to ozone absorption at 500 nm (τ_o), according to the formulation by Dutton et al. (1994), were 0.009 on 13 April, and 0.008 on 17 April.

Because of the poor air quality on 13 and 17 April, absorption by NO_2 was also considered. Surface concentrations of NO_2 sampled by the Colorado Department of Public Health and the Environment were obtained for four sites in the Denver metropolitan area. The closest sampling station to Boulder was 10 km south of the city. To maximize the results, the highest hourly value among the four stations for a particular day was chosen to represent the NO_2 concentration of the entire region, and the boundary layer depth used was the highest observed on that day according to the Denver rawinsonde. It should be noted that the sampling station closest to Boulder never had the highest NO_2 concentration. The highest τ_N computed for the Denver metropolitan area for 13 April 2001 was 0.005 at 1100 LST, and that for 17 April was 0.001 between 1200 and 1400 LST. Given that these values represent the absolute maximum contributions by NO_2 that could have occurred on these 2 days, and that they would have only been achieved for very short periods, the NO_2 contribution to the total optical depth was neglected.

c. Error assessment

The calibration $I_{\lambda 0}$ was applied to 500-nm MFRSR measurements on 13 and 17 April to provide time series of total optical depth. Errors in the retrieved total optical depths related to the calibration method were assessed by applying the standard deviation of the mean $\ln(I_{\lambda 0})$ to the time series of two-point slope calculations. The standard deviation (0.057) was added to the mean $\ln(I_{\lambda 0})$ to provide an upper limit $\ln(I_{\lambda 0})$, and a lower limit $\ln(I_{\lambda 0})$ was computed by subtracting the standard deviation from the mean. The total optical depth time series was recomputed twice using the upper and lower limit $\ln(I_{\lambda 0})$ values. For both days, differences between these total optical depths and those computed using the mean $\ln(I_{\lambda 0})$ ranged from ± 0.01 in the morning and evening (large solar zenith angles) to ± 0.05 near midday (small solar zenith angles). The magnitudes of these errors could be reduced by applying statistical elimination logic to the sample of $\ln(I_{\lambda 0})$ values used to compute the mean, as in Michalsky et al. (2001). Therefore, the reported method-related errors represent a worst-case scenario for retrieved total optical depths for the two high air pollution days.

Any errors associated with the computation of τ_R, τ_N, and τ_o must be added to the method-related errors because they are independent of the calibration procedure. Errors associated with the calculation of molecular scattering and ozone absorption for this application were assessed by varying parameters used to compute them

through typical ranges observed at Table Mountain. The optical depth due to ozone absorption (τ_o) at 500 nm was computed for 250 and 400 Dobson units, and that attributed to molecular scattering was computed for the average surface pressure at Table Mountain (835 hPa) $\pm$20 hPa. Resultant variations of τ_o and τ_R for those ranges were in the thousandths decimal place. When rounded to the nearest hundredth, which is the accuracy of the AOD values reported here, all values for τ_o and τ_R in these tests were identical to the values used in this application, that is, 0.01 and 0.12. Thus, when reporting AOD to the hundredths place, errors in the station pressure and total ozone used to compute τ_R and τ_o will have little, or as in this case, no effect on the accuracy of the retrieved AOD.

d. Aerosol optical depths for 13 and 17 April 2001

The AOD results for 13 and 17 April are presented in Fig. 6. The highest values on 13 April (Fig. 6a) of $>$0.30 occurred in the early morning, after which the AOD dropped off sharply to less than 0.20 by midmorning. It gradually fell to near-background levels by midday, suggesting that the capping inversion eroded during the morning, allowing the westerly winds aloft to mix downward and disperse or advect away the surface-based aerosols. The AOD gradually increased through the afternoon on 13 April, reached a short-lived peak of about 0.25 at 1545 LST, then decreased to less than 0.20 in the late afternoon. Intermittent spikes of erroneously high AOD values in the afternoon and in the last part of the analysis period in Fig. 6a indicate contamination by clouds and should be ignored. This contamination is also apparent in the early part of 17 April (Fig. 6b), but at about 1000 LST the clouds disappear. This clearing was confirmed with the aid of 1-min hemispheric sky images from the Total Sky Imager at the Table Mountain SURFRAD station. During the remainder of 17 April, AOD values ranged from approximately 0.40 in the morning to about 0.30 in late afternoon, substantially higher than the background level of 0.12. These high AODs are consistent with the meteorological conditions that acted to trap aerosols close to the surface on that day.

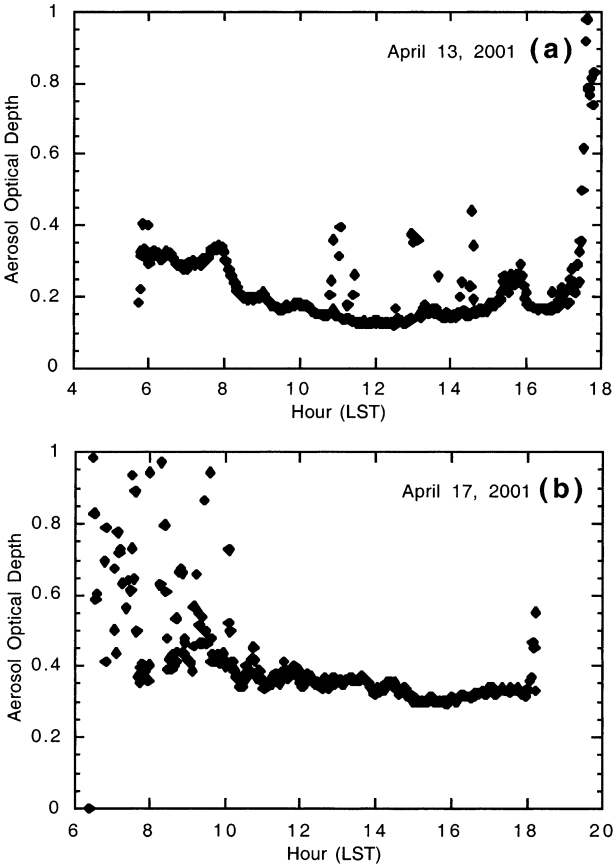

FIG. 6. Time series of aerosol optical depth for Table Mountain on (a) 13 and (b) 17 Apr 2001. Anomalous spikes in the time series represent contamination in the measurements that is likely caused by clouds and should be ignored.

e. Comparison with other AOD measurements

The only other available AOD measurements in northeastern Colorado on 13 and 17 April 2001 were at the USDA UV monitoring station at the Pawnee National Grasslands 85 km northeast of the Table Mountain SURFRAD station, and at DOE's National Renewable Energy Laboratory (NREL) in Golden, Colorado, which is 50 km south of the SURFRAD station. Figure 4 shows the geographical distribution of the three stations. The Pawnee site has an MFRSR, and NREL employs an automated 500-nm sun photometer. The USDA calibrates their Pawnee MFRSR for AOD using the method described in Harrison and Michalsky (1994). Comparisons of AOD measurements between Table Mountain and the other two stations for 13 April are shown in Fig. 7, and those for 17 April are shown in Fig. 8. Only synchronized measurements are compared; no interpolation was done to match these datasets.

By the close agreement seen in Fig. 7a, it is obvious that the Pawnee and Table Mountain MFRSRs were sampling similar atmospheric conditions on 13 April when the upper-level Asian dust cloud was over Colorado. However, Fig. 7b shows that measurements at NREL in Golden agree only briefly with those at Table Mountain in the early morning just before 0800 LST, and in the late afternoon between 1500 and 1600 LST. At other times during that day, AOD measurements at NREL are approximately 0.10 higher than those at Table Mountain. Spatial variations in the Asian dust cloud may explain this difference; however, the NAAPS imagery is too coarse to be able to discern such a variation between Golden and Table Mountain. The explanation for this discrepancy may lie in the closer proximity of Golden to Denver's urban aerosol plume.

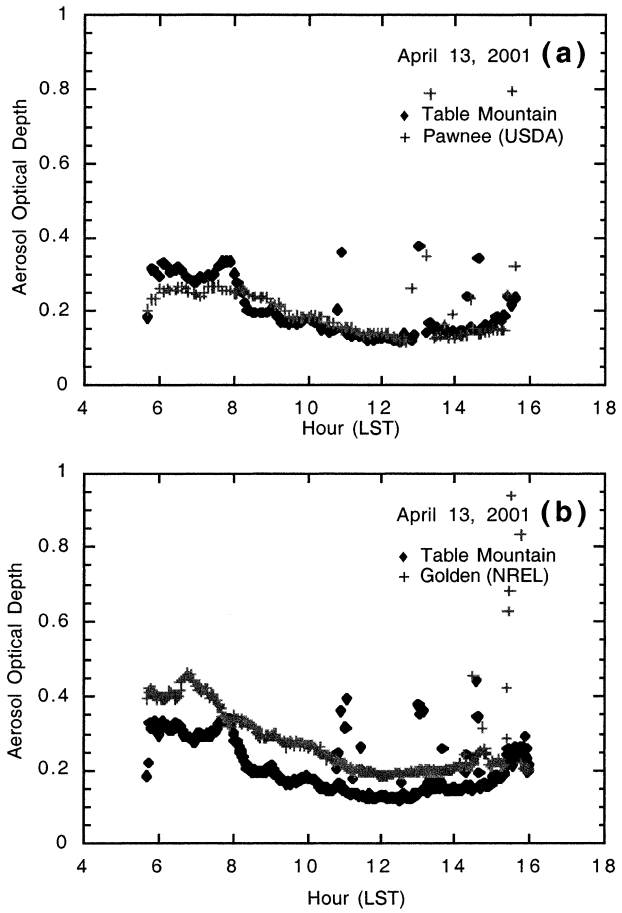

FIG. 7. Comparisons of aerosol optical depth time series for 13 Apr 2001 between (a) Table Mountain (♦) and the USDA station at the Pawnee National Grasslands (+), and (b) Table Mountain (♦) and the NREL station in Golden, CO (+). As in Fig. 6, anomalous spikes in the time series likely represent cloud contamination and should be ignored.

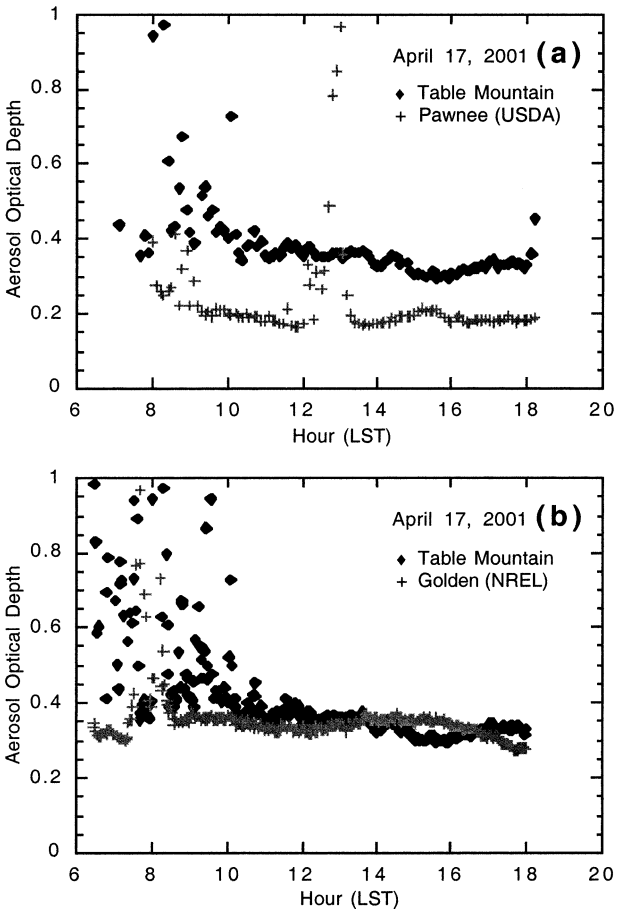

FIG. 8. Same as in Fig. 7 but for 17 Apr 2001.

On 17 April, AOD values at Table Mountain are approximately twice those at Pawnee (Fig. 8a), but the NREL and Table Mountain measurements agree quite well throughout the day (Fig. 8b). Weather conditions on 17 April, and the relative locations of the three stations may explain these differences. Light south-southeast surface winds in eastern Colorado emanating from the surface high pressure area to the east would push surface aerosols toward the west, concentrating highly polluted air against the Front Range and under the low-level inversion, resulting in a west-to-east gradient in aerosol concentration. This scenario is corroborated by the NAAPS imagery, which shows surface aerosols concentrated along the eastern side of the Front Range of the Rocky Mountains in Colorado throughout the day. The fact that the Table Mountain SURFRAD station and NREL are just a few kilometers east of the Front Range reasonably explains why these two stations show high aerosol loadings on 17 April. In contrast, the Pawnee station is on the eastern plains, away from the combined trapping effects of the low-level inversion and the Front Range, and therefore exhibits lower aerosol amounts.

Aerosol optical depth measurements from the AERONET network for 10–25 April 2001 are reported by Thulasiraman et al. (2002). The nearest reporting AERONET stations to Colorado in April 2001 were Missoula, Montana, 966 km to the northwest of Table Mountain, and Bondville, Illinois, 1435 km to the east. Given the trajectory of the Asian dust plume in the NAAPS imagery, it would have affected Montana first, then Colorado, and then Illinois. Values of AOD ranging from <0.2 to 0.4 were observed at Missoula on 16 April, a day before a maximum in the Asian dust plume reached Colorado. A 10-day gap in the Missoula AOD time series prior to 15 April precludes such a comparison for the 13 April event in Boulder. At Bondville, Illinois, the AERONET time series shows two AOD maxima greater than 0.4 on 14–15 April, and on 18–19 April, which are a day or two after corresponding maxima were observed in Colorado. The magnitudes and timing of these three sets of AOD observations are

consistent with the documented trajectory of the plume across North America.

f. Effects of the aerosols on the surface radiation

The Long and Ackerman (2000) clear-sky analysis results for 13 and 17 April present the opportunity to compare the actual solar measurements with normally expected clear-sky values for those days. During the afternoon of 17 April, when no clouds were present, the dust-laden boundary layer air reduced the direct solar signal at the surface by 15%–20%, and increased the diffuse signal by 50%–100% over normally expected clear-sky amounts. These opposing effects nearly cancel, resulting in only a 4%–8% net reduction in the total solar irradiance received at the surface. On 13 April, the effects of the dust on the surface solar irradiance varied over the course of the day as characteristics of the boundary layer changed. For short periods in the early morning and late afternoon, aerosols reduced the direct solar irradiance at the surface by 5%–10% and increased the diffuse irradiance by 60%–100% over normally expected clear-sky amounts. In contrast, at midday, when the AOD was at its low point (Fig. 6a), the reduction of the direct signal was only a few percent and the increase in diffuse irradiance amounted to only 10%. At that time, these effects combined to produce a 2% increase in the total solar radiation over that expected under clear skies.

g. Comparison with the Asian dust event of April 1998

In nearly identical circumstances as in April 2001, intense storms over Mongolia and northern China in April 1998 swept Gobi Desert dust into the atmosphere that was transported across the Pacific Ocean to North America. Husar et al. (2001) reported that in the western United States the desert dust reduced the direct solar irradiance by 30% to 40%, and increased the diffuse solar signal by a factor of 2, relative to typical clear-sky values. They also report average AOD measurements of 0.40 at Reno, Nevada, and in the Pacific Northwest. These characteristics of the April 1998 Asian dust episode are similar to those reported here for 13 and 17 April 2001.

7. Summary and conclusions

Networks of Multifilter Rotating Shadowband Radiometers (MFRSR) and automated sun photometers established over the last decade in the United States have led to a resurgence of aerosol optical depth (AOD) information. Unlike the manually operated Volz sun photometers of the 1960s, MFRSRs operate remotely and continuously during the daylight hours. Owing to their ''blind'' operation, the selection of suitable data for Langley plot calibration requires extensive screening and quality control. Here, we introduce the method whereby the automated algorithm of Long and Ackerman (2000) is used to identify cloud-free and nonhazy periods. Spectral MFRSR data corresponding to the clear periods are used to construct a set of calibration Langley plots. Because these plots represent only cloud-free periods, they exhibit little scatter and produce reliable extrapolations to zero air mass, or the extraterrestrial signal ($I_{\lambda 0}$). A representative $I_{\lambda 0}$ for a several-week calibration period is computed by averaging the extrapolated clear-sky $I_{\lambda 0}$ values. This mean, or calibration $I_{\lambda 0}$, may then be applied to any I_{λ} measurement within the calibration period to compute aerosol optical depth.

To test this process, the clear-sky identification method was applied 2 months of Table Mountain SURFRAD solar broadband component data from late March through late May of 2001. Clear-sky periods from these days included 13 mornings and 5 afternoons, from which 18 calibration Langley plots were produced. Because the clear-sky Langley plots include only cloud-free and nonhazy periods, their mean slope (total optical depth), minus the effects of molecular scattering and ozone absorption, of 0.12 represents the background AOD for the calibration period.

The $I_{\lambda 0}$ calibration value was applied to the Table Mountain SURFRAD MFRSR 500-nm channel data for two high air pollution events that occurred in Boulder, Colorado, on 13 and 17 April 2001. Both were associated with a plume of desert dust from Asia. The upper-level dust cloud was over Colorado on 13 April, but on 17 April the dust was only present at the surface. Retrieved AODs for 17 April ranged from about 0.30 to near 0.40, and those for 13 April ranged from >0.3 in the morning to near-background levels in the afternoon. The higher AOD values on 17 April were consistent with meteorological conditions favorable for trapping aerosols close to the surface and against the Front Range of the Rocky Mountains on that day.

Corroboration for our calculations was found in independent MFRSR-based AOD measurements at the USDA station at the Pawnee National Grasslands 85 km to the northeast of Table Mountain, and sun-photometer-based AOD measurements made at NREL in Golden, Colorado, 50 km to the south of the SURFRAD station. Both NREL and Table Mountain are close to the mountains, whereas Pawnee is on the eastern plains. On 17 April, when greater surface aerosol concentrations were favored along the Front Range, AODs at Table Mountain and NREL were similar, but they were about 2 times the magnitude of those at Pawnee. On 13 April, when the upper-level Asian dust cloud enveloped Colorado, the AOD time series at Table Mountain and Pawnee compared well, but the measurements at NREL in Golden were generally higher by 0.05–0.10. This discrepancy could not be definitively explained, but the proximity of Golden to Denver's urban aerosol plume may be the source of the difference.

It has been shown that the clear-sky identification method of Long and Ackerman (2000) is a useful tool for selecting periods of MFRSR data appropriate for Langley plot calibration. Because this method is automated, its use as a screening aid for MFRSR spectral channel calibration data represents an improvement in the efficiency of MFRSR-based AOD analyses. Here, collocated independent SURFRAD broadband solar component measurements were used for the clear-sky determination, and those results were then used to select MFRSR measurements for $I_{\lambda 0}$ calibration. However, having collocated independent broadband solar measurements is not necessary if an MFRSR's broadband solar channel is nominally calibrated. The Long and Ackerman method has been successfully applied to absolutely calibrated MFRSR broadband data at the Pacific Northwest National Laboratory. These results suggest that the method presented is applicable to stand-alone MFRSRs presently operating in the United States, as long as some effort is directed to calibrating their broadband channels.

Acknowledgments. This research was made possible through the generosity of the NASA EOS program, particularly David Starr, Bruce Barkstrom, and Bruce Wielicki. The measurements used in this work would not have been possible without the support of NOAA's Office of Global Programs who recognized the need for high-quality surface radiation budget measurements in the United States by funding the SURFRAD network. The SURFRAD program is also indebted to Joe Michalsky (Quantitative Links Program) and the USDA Ultraviolet Radiation Monitoring Program for sharing their MFRSR data. The authors express their appreciation to Jim Slusser at Colorado State University, and to Tom Stoffel and Daryl Myers at DOE's National Renewable Energy Laboratory for providing the aerosol optical depth validation data. Recognition is also due to the Colorado Department of Public Health and the Environment for providing NO_2 data, to NOAA/CMDL for sharing their total ozone measurements for Boulder, and to the Naval Research Laboratory for making the NAAPS aerosol distribution maps available on the Internet. We would also like to thank Amy Stevermer who capably assisted in editing the manuscript, and Ellsworth Dutton and Irina Petropavlovskikh for sharing their expertise. Last, the authors are most grateful for useful comments made by the anonymous reviewers, which improved the quality of this manuscript.

REFERENCES

Alexandrov, M. D., A. A. Lacis, B. E. Carlson, and B. Cairns, 2002: Remote sensing of atmospheric aerosols and trace gases by means of Multifilter Rotating Shadowband Radiometer. Part I: Retrieval algorithm. *J. Atmos. Sci.,* **59,** 524–543.

Augustine, J. A., J. J. DeLuisi, and C. N. Long, 2000: SURFRAD—a national surface radiation budget network for atmospheric research. *Bull. Amer. Meteor. Soc.,* **81,** 2341–2357.

Bigelow, D. S., J. R. Slusser, A. F. Beaubien, and J. H. Gibson, 1998: The USDA Ultraviolet Radiation Monitoring Program. *Bull. Amer. Meteor. Soc.,* **79,** 601–615.

Charlson, R. J., S. E. Schwartz, J. M. Hales, R. D. Cess, J. A. Coakley, J. E. Hansen, and D. J. Hofmann, 1992: Climate forcing by anthropogenic aerosols. *Science,* **255,** 423–430.

Davidson, J. A., C. A. Cantrell, A. H. McDaniel, R. E. Shetter, S. Madronich, and J. G. Calvert, 1988: Visible-ultraviolet absorption cross sections for NO_2 as a function of temperature. *J. Geophys. Res.,* **93** (D6), 7105–7112.

Dutton, E. G., and J. R. Christy, 1992: Solar radiative forcing at selected locations and evidence for global lower tropospheric cooling following the eruptions of El Chichon and Pinatubo. *Geophys. Res. Lett.,* **19,** 2313–2316.

——, P. Reddy, S. Ryan, and J. J. DeLuisi, 1994: Features and effects of aerosol optical depth observed at Mauna Loa, Hawaii: 1982–1992. *J. Geophys. Res.,* **99** (D4), 8295–8306.

Flowers, E. C., R. A. McCormick, and K. R. Kurfis, 1969: Atmospheric turbidity over the United States, 1961–1969. *J. Appl. Meteor.,* **8,** 955–962.

Forgan, B. W., 1988: Sun photometer calibration by the ratio Langley method. *Baseline Atmospheric Program,* B. W. Forgan and P. J. Fraser, Eds., Bureau of Meteorology, 22–26.

Hansen, J., A. Lacis, R. Ruedy, and M. Sato, 1992: Potential climate impact of Mount Pinatubo eruption. *Geophys. Res. Lett.,* **19,** 215–218.

——, M. Sato, R. Ruedy, A. Lacis, and V. Oinas, 2000: Global warming in the twenty-first century: An alternative scenario. *Proc. Natl. Acad. Sci. USA,* **97,** 9875–9880.

Harrison, L., and J. Michalsky, 1994: Objective algorithms for the retrieval of optical depths from ground-based measurements. *Appl. Opt.,* **33,** 5126–5132.

——, ——, and J. Berndt, 1994: Automated multifilter rotating shadow-band radiometer: An instrument for optical depth and radiation measurements. *Appl. Opt.,* **33,** 5118–5125.

Holben, B. N., and Coauthors, 2001: An emerging ground-based aerosol climatology: Aerosol optical depth from AERONET. *J. Geophys. Res.,* **106** (D11), 12 067–12 097.

Husar, R. B., and Coauthors, 2001: Asian dust events of April 1998. *J. Geophys. Res.,* **106** (D16), 18 317–18 330.

Long, C. N., and T. P. Ackerman, 2000: Identification of clear skies from broadband pyranometer measurements and calculation of downwelling shortwave cloud effects. *J. Geophys. Res.,* **105** (D12), 15 609–15 626.

Marggraf, W. A., and M. Griggs, 1969: Aircraft measurements and calculations of the total downward flux of solar radiation as a function of altitude. *J. Atmos. Sci.,* **26,** 469–477.

Michalsky, J. J., J. A. Schlemmer, W. E. Berkheiser, J. L. Berndt, and L. C. Harrison, 2001: Multiyear measurements of aerosol optical depth in the Atmospheric Radiation Measurement and Quantitative Links programs. *J. Geophys. Res.,* **106** (D11), 12 099–12 107.

Parungo, F., Z. Li, X. Li, D. Yang, and J. Harris, 1994: Gobi dust storms and The Great Green Wall. *Geophys. Res. Lett.,* **21,** 999–1002.

Reagan, J. A., I. C. Scott-Fleming, B. M. Herman, and R. M. Schotland, 1984: Recovery of spectral optical depth and zero airmass solar spectral irradiance under conditions of temporarily varying optical depth. *Proc. Int. Geoscience and Remote Sensing Symp.,* Strasbourg, France, European Space Agency, 455–459.

Shaw, G. E., 1976: Error analysis of multi-wavelength sun photometry. *Pure Appl. Geophys.,* **114,** 1–14.

——, 1983: Sun photometry. *Bull. Amer. Meteor. Soc.,* **64,** 4–10.

Smith, F. L., III, and C. Smith, 1972: Numerical evaluation of Chapman's grazing incidence integral ch(X, χ). *J. Geophys. Res.,* **77,** 3592–3597.

Stokes, G. M., and S. E. Schwartz, 1994: The Atmospheric Radiation

Measurement (ARM) Program: Programmatic background and design of the cloud and radiation test bed. *Bull. Amer. Meteor. Soc.,* **75,** 1201–1221.

Thulasiraman, S., N. T. O'Neill, A. Royer, B. N. Holben, D. L. Westphal, and L. J. B. McArthur, 2002: Sunphotometric observations of the 2001 Asian dust storm over Canada and the U.S. *Geophys. Res. Lett.,* **29,** 96.1–96.4.

Uematsu, M., R. A. Duce, J. M. Prospero, L. Chen, J. T. Merrill, and R. L. McDonald, 1983: Transport of mineral aerosol from Asia over the North Pacific Ocean. *J. Geophys. Res.,* **88,** 5343–5352.